Three-dimensional maps of the tomographic incompleteness of cone-beam CT scanner geometries

Matthieu Laurendeau, Laurent Desbat, Guillaume Bernard, Frédéric Jolivet, Sébastien Gorges, Fanny Morin, Simon Rit

Three-dimensional maps of the tomographic incompleteness of cone-beam CT scanner geometries

Matthieu Laurendeau[1,2,3], Laurent Desbat[1], Guillaume Bernard[2], Frédéric Jolivet[2], Sébastien Gorges[2], Fanny Morin[2], and Simon Rit[3]

[1]Univ. Grenoble Alpes, CNRS, UMR 5525, VetAgro Sup, Grenoble INP, TIMC, 38000 Grenoble, France
[2]Thales AVS, Moirans, France
[3]Univ Lyon, INSA-Lyon, Université Claude Bernard Lyon 1, UJM-Saint Étienne, CNRS, Inserm, CREATIS UMR 5220, U1294, F-69373, Lyon, France

Abstract New generations of X-ray sources based on carbon nanotubes (CNT) enable the design of multi-sources computed tomography (CT) scanners. CT scanners with CNT often use a limited number of stationary sources and corresponding projections. Three-dimensional CT theory evaluates whether a given continuous source trajectory provides sufficient data for stable reconstruction of an imaged object. This paper extends a local incompleteness metric to derive a three-dimensional map and quantify tomographic incompleteness for a finite set of sources. We illustrate this incompleteness with a dedicated phantom. The reconstructed CT images of the phantom match the results predicted by the incompleteness map.

Keywords X-ray cone-beam CT; Stationary architecture; Tomographic incompleteness

1 Introduction

Computed tomography (CT) is one of the most commonly used imaging modality for three-dimensional (3D) reconstruction in the medical and industrial fields. In the past few years, new X-ray sources have been developed based on carbon nanotube (CNT) cathodes [1]. Their small size enables the design of a new generation of CT scanners. It would benefit both industry with cheaper and motionless systems and medical applications with light-weight and mobile scanners which could be brought to emergency sites.

In a 3D context, CT scanners can be split into two categories: non-stationary architectures with mobile source(s) and stationary architectures with static source(s). Non-stationary architectures are the most common ones with source trajectories such as the conventional helix path or the circle-line path [2] which is adapted to C-arm scanners. Micro CNTs have opened new horizons for CT scanners with stationary architectures. The idea is to place several stationary sources around the scanned area. Gonzales *et al.* [3] and Vogtmeier *et al.* [4] have proposed two stationary designs for controlling luggage at airports.

3D CT theory has a few tools to help with the geometrical design of a CT scanner. Assuming non-truncated projections, Tuy [5] gave a condition to verify if a continuous source trajectory is sufficient to reconstruct an open region Ω. The condition can be stated as: *every plane that intersects the imaged region* Ω *must intersect the scanning trajectory at least once*. In practice, all scanners are limited by a finite set of source locations instead of a continuous curve and Tuy's condition is never strictly satisfied. However, it is known that discrete sampling of a helical trajectory allows stable reconstruction.

Several metrics have been studied to quantify the impact of tomographic incompleteness, i.e. when Tuy's condition is not met. Metzler *et al.* [6] and Lin and Meikle [7] calculate a voxel-based percentage considering the unit sphere by locally linking Orlov's and Tuy's conditions [6]. Their metric is similar to that of Liu *et al.* [8] which was derived from the theory of the 3D Radon transform. They numerically evaluate the fraction of planes which are intersected by the source trajectory by sampling the unit sphere. This kind of measure is only possible for continuous source trajectories and the authors indicate that it is difficult to predict the reconstruction quality from this metric as, for example, 99% may lead to poorer image quality than 96%. Clackdoyle and Noo [9] quantify tomographic incompleteness to measure how far a voxel is from locally satisfying Tuy's condition in a given direction. Stopp *et al.* [10] proposed to average a similar measure in all directions. These last two criteria can be applied to both continuous and discrete source trajectories.

Our work aims at evaluating tomographic incompleteness for the design of new CT scanners assuming (first) non-truncated projections. We build on the quantification of tomographic incompleteness [9] to predict the worst direction in each spatial position of a 3D map. For four selected geometries, we demonstrate the relevance of this quantification by reconstructing a phantom made of three parallel cylinders placed at the worst location and oriented in the worst direction according to the incompleteness map.

2 Materials and Methods

2.1 Source trajectories

The incompleteness map is computed for a given source trajectory. We have chosen to compute it for four discrete geometries assuming that the imaged object is contained in the same 256^3 mm^3 cube for all geometries. Fig. 1 illustrates the trajectories from the object point of view and Tab. 1 provides key parameters of each geometry. The first two architectures are conventional non-stationary architectures: circle-line and helix. The circle only satisfies Tuy's condition in the trajectory plane. We have selected the circle-line among several variants to extend the reconstructible region [2]. Here, we study the discrete form of this geometry and place the line

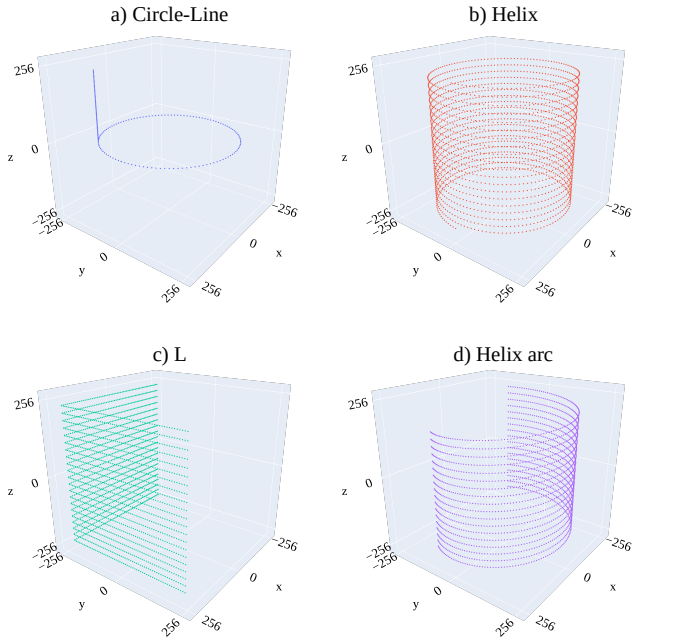

Figure 1: The four geometries studied in the object's coordinate system. a) combines a circle, which allows stable reconstruction only in its plane, with an orthogonal line above to complete data in the superior half of the object. The imaged object translates in the z direction for the b), c) and d) geometries. b) consists of a source with a circle path which makes it a helix when the object translates axially. c) has an L shape with sources placed on two orthogonal segments which are repeated when the imaged object moves. In d), sources are located on a helix arc and are duplicated in the axial direction.

Table 1: Key parameters of the four source trajectories.

	Object translation (mm/cycle)	Sources	Radius (mm)	Special attributes (mm)
Circle-line	None	120 (C) + 60 (L)	240 (360°)	line height: 240
Helix	[0,0,24]	120 x 20 cycles	240 (360°)	
L	[0,0,24]	120 x 21 cycles	240 (straight)	
Helix arc	[0,0,24]	120 x 18 cycles	240 (245°)	helical pitch: 120

above the circle only. In this context, Tuy's condition is not satisfied below the circle and the incompleteness should be lower above it. The helix source path is the geometry of most diagnostic CT scanners. It is composed of a source following a circle path while the imaged object translates axially through the circle which results in a helix in the coordinate system of the scanned object. For a continuous source curve, Tuy's condition is satisfied, and we anticipate a very low incompleteness for a finite set of source points.

The other two architectures are stationary: L and helix arc. The L geometry was one of the first stationary architecture commercialized for airport security [3]. It is made of two segments of sources which leaves space for detectors on the opposite side. The helix arc places sources along an arc of helix. For these two geometries, the imaged object is translated through the gantry. From the object's point of view, the pattern of sources is repeated according to the object motion in several identical cycles.

2.2 Tomographic incompleteness

Clackdoyle and Noo [9] defined their local directional incompleteness criterion $\mathrm{I}(\mathbf{x},\ \mathbf{n}) \in \mathbb{R}^+$ at $\mathbf{x} \in \Omega \subset \mathbb{R}^3$ in the direction $\mathbf{n} \in S^2$, where S^2 is the unit sphere, for a source trajectory $\{\mathbf{s}_1, \mathbf{s}_2, ..., \mathbf{s}_n\} \in \mathbb{R}^{3\times n}$ as following:

$$\mathrm{I}(\mathbf{x},\mathbf{n}) = \min\left\{\frac{||\mathbf{s}_i - \mathbf{p}_i||}{||\mathbf{x} - \mathbf{p}_i||} : i = 1,2,...,n\right\} \tag{1}$$

where $\mathbf{p}_i \in \mathbb{R}^3$ is the projection of the source $\mathbf{s}_i$ onto the plane $\Pi_{\mathbf{x},\mathbf{n}}$ passing through the point $\mathbf{x}$ and of normal direction $\mathbf{n}$:

$$\mathbf{p}_i = \mathbf{s}_i - ((\mathbf{s}_i - \mathbf{x}) \cdot \mathbf{n})\mathbf{n}. \tag{2}$$

This criterion evaluates the minimum tangent of the angles defined by the plane $\Pi_{\mathbf{x},\mathbf{n}}$ and the X-ray lines, i.e. the lines passing through the point $\mathbf{x}$ and the source positions along the trajectory. If $\mathrm{I}(\mathbf{x},\mathbf{n}) = 0$, the plane cuts the source trajectory. Therefore, if $\mathrm{I}(\mathbf{x},\mathbf{n}) = 0$ for all $\mathbf{n} \in S^2$, the point $\mathbf{x}$ satisfies Tuy's condition and can be reconstructed if the acquired projections are not truncated. If $\mathrm{I}(\mathbf{x},\mathbf{n}) > 0$, the plane with co-direction $\mathbf{n}$ does not intersect the source trajectory and the point $\mathbf{x}$ does not satisfy Tuy's condition.

We use this criterion to evaluate the 3D spatial distribution of the tomographic incompleteness in the imaged region Ω. Since we aim at identifying the less complete location and direction, we only record the maps of the worst directions $\mathbf{n}_\infty : \Omega \to S^2$

$$\mathbf{n}_\infty(\mathbf{x}) = \underset{\mathbf{n}\in S^2}{\arg\max}\{\mathrm{I}(\mathbf{x},\mathbf{n})\} \quad \forall\, \mathbf{x} \in \Omega \tag{3}$$

and the corresponding incompleteness $\mathrm{I}_\infty : \Omega \to \mathbb{R}^+$

$$\mathrm{I}_\infty(\mathbf{x}) = \mathrm{I}(\mathbf{x},\mathbf{n}_\infty(\mathbf{x})) \quad \forall\, \mathbf{x} \in \Omega. \tag{4}$$

In practice, $\mathbf{n}_\infty$ and I_∞ are computed numerically by discretizing both the unit sphere S^2 and the object space Ω. A unit hemisphere is sufficient due to the symmetry $\mathrm{I}(\mathbf{x},-\mathbf{n}) = \mathrm{I}(\mathbf{x},\mathbf{n})$. We sampled 3000 directions using Fibonacci lattice method [11]. Fibonacci lattice arranges points along a spherical spiral homogeneously. Iteratively, each new point is placed evenly between the largest gap of the previous points.

2.3 Simulation phantom

To verify the incompleteness map, we simulated noiseless and untruncated projections for each geometry with a dedicated phantom. The phantom was made of three parallel cylinders with a 24 mm radius, a 6 mm height and a center-to-center distance of 6 mm. According to the incompleteness result of each geometry, the phantom's center was placed at the worst position in the subregion $\tilde{\Omega} \subset \Omega$ which can fully contain the phantom

$$\mathbf{x}^* = \underset{\mathbf{x}\in\tilde{\Omega}}{\arg\max}\{\mathrm{I}_\infty(\mathbf{x})\} \tag{5}$$

and in the worst direction $\mathbf{n}^* \in S^2$

$$\mathbf{n}^* = \mathbf{n}_\infty(\mathbf{x}^*). \tag{6}$$

CT images were reconstructed with RTK [12] using a least-squares iterative reconstruction with conjugate gradient minimization without regularization. We used 60 iterations which was visually deemed a good compromise between convergence, overfitting and image quality.

3 Results

3.1 Tomographic incompleteness map

Fig. 2 shows the incompleteness map of each studied geometry. It is a combination of the result of Eq. 3 and Eq. 4 for a given imaged region and source trajectory. In each position $\mathbf{x}$ of the imaged region, the value $\mathrm{I}_\infty(\mathbf{x})$ and the worst direction associated $\mathbf{n}_\infty(\mathbf{x})$ are calculated. The map illustrates both information using colors and 3D cones respectively.

The incompleteness maps of the circle-line and helix trajectories confirm the well known theory. For the circle-line trajectory, the incompleteness is low in the convex hull of the trajectory, $\min\{\mathrm{I}_\infty(\mathbf{x})\} \simeq 0.016$. However, below the circle plane, the imaged region is not reconstructible which translates into high incompleteness values $\max\{\mathrm{I}_\infty(\mathbf{x})\} \simeq 0.675$. The worst direction $\mathbf{n}^*$ at the bottom is almost orthogonal to the circle plane, as expected since the plane $\Pi_{\mathbf{x}^*,\mathbf{n}^*}$ is parallel to the trajectory circle and is not intersecting it nor the trajectory line. The helix's map displays a small incompleteness everywhere, $0.005 \leq \mathrm{I}_\infty(\mathbf{x}) \leq 0.016$. The residual incompleteness stems from the helix sampling.

For stationary architectures, the L trajectory is incomplete at the opposite of the two rectangles of sources with $\max\{\mathrm{I}_\infty(\mathbf{x})\} \simeq 0.456$. In this case, the worst direction $\mathbf{n}^*$ defines a plane parallel to the convex hull of the trajectory, which is consistent with Tuy's criterion. Near the sources, the incompleteness is small $\min\{\mathrm{I}_\infty(\mathbf{x})\} \simeq 0.006$, as expected, and the direction depends on the source sampling. Finally, the incompleteness map of the helix arc is similar to the non-stationary helix due to their similar trajectories: $0.005 \leq \mathrm{I}_\infty(\mathbf{x}) \leq 0.030$. It proves that a stationary design can compete with non-stationary architectures if a similar number of source locations is used.

3.2 Simulation & Reconstruction

The simulated 3D phantom of three parallel cylinders is placed at the worst position $\mathbf{x}^*$ (Eq. 5) and in the worst direction $\mathbf{n}^*$ (Eq. 6) in $\tilde{\Omega}$ for each geometry. The reconstructed images are shown in Fig. 3 such that the phantom is centered with $\mathbf{n}^*$ vertical.

The helix and helix arc trajectories have good image quality as predicted by their respective incompleteness maps. The circle-line trajectory has the worst image quality, and it is difficult to separate the cylinders. Finally, the L reconstruction has a slightly better image quality than the circle-line trajectory, but it is also difficult to distinguish the three cylinders.

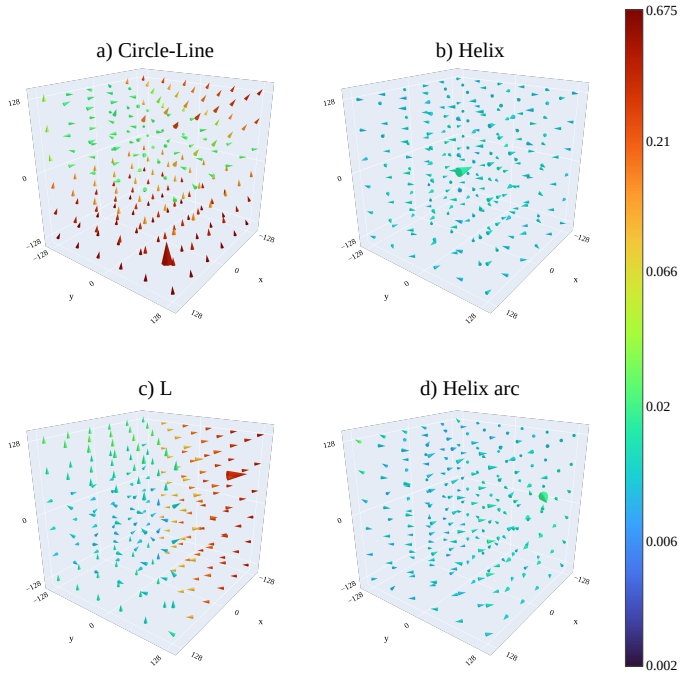

Figure 2: Tomographic incompleteness maps of the four studied geometries. Each map is centered on the imaged region Ω (ratio $1/2$ in each direction with respect to Fig. 1 and the same camera angle). The direction and the color of each cone represent the worst direction $\mathbf{n}_\infty(\mathbf{x})$ (Eq. 3) and the corresponding incompleteness $\mathrm{I}_\infty(\mathbf{x})$ (Eq. 4), respectively. The bigger cone shows the worst position $\mathbf{x}^*$ (Eq. 5) in the worst direction $\mathbf{n}^*$ (Eq. 6) in $\tilde{\Omega}$.

4 Discussion

The incompleteness map presented in this work accurately predicts image quality of a dedicated phantom. The incompleteness map is based on Tuy's theory and assumes untrucated projections. Accounting for the truncation of the projections was beyond the scope of this work.

The computation of the worst directions $\mathbf{n}_\infty$ was done numerically by sampling the unit sphere. The sampling pattern [11] was selected because it homogeneously samples the sphere. We took about 3000 points on the hemisphere which does not warrant to find the worst direction. However, the incompleteness maps I_∞ and $\mathbf{n}_\infty$ are quite smooth, at least for larger values which are not influenced by the trajectory sampling, and this discretization of the unit sphere may be sufficient to have a good estimate of $\mathbf{n}_\infty$. Finally, it is common for stationary architectures to use iterative reconstruction algorithms. We have chosen to use the same iterative algorithm, without regularization but a fixed number of iterations, which provides a quite fair comparison of all geometries.

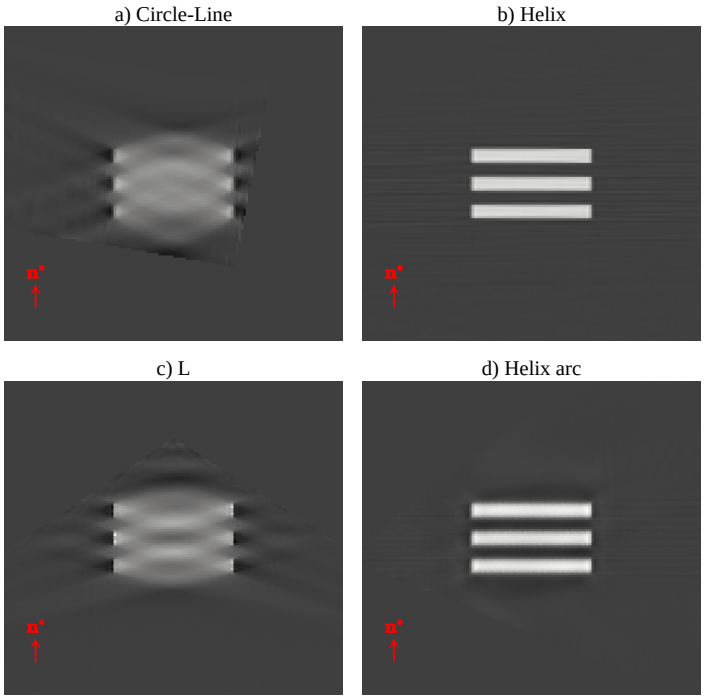

Figure 3: Least squares reconstruction of the same phantom for each geometry. The phantom is composed of three parallel cylinders and, for each geometry, it is placed at the worst position $\mathbf{x}^*$ (provided by Eq. 5) and in the worst direction $\mathbf{n}^*$ (provided by Eq. 6) in $\tilde{\Omega}$, as shown with a bigger cone in Fig 2. For comparison purposes, we have registered the reconstructed images to place the phantom in the center and such that $\mathbf{n}^*$ is vertical.

5 Conclusion

Our work defines the tomographic incompleteness map which was computed on four architectures: two non-stationary and two stationary. We have chosen a similar number of sources, radius and other characteristics to make them comparable. The results show that the incompleteness map is in agreement with Tuy's theory (on which it is based). These maps adequately predict the image quality of a dedicated disk phantom scanned at the worst location and in the worst direction provided by the incompleteness map. The incompleteness map may be used to design a compact geometry scanner with a limited number of sources by minimizing the incompleteness value in a scanned region.

References

[1] R. J. Parmee, C. M. Collins, W. I. Milne, et al. "X-ray generation using carbon nanotubes". *Nano Convergence* 2.1 (2015). DOI: 10.1186/s40580-014-0034-2.

[2] G. L. Zeng and G. T. Gullberg. "A cone-beam tomography algorithm for orthogonal circle-and-line orbit". *Physics in Medicine and Biology* 37.3 (1992), pp. 563–577. DOI: https://doi.org/10.1088/0031-9155/37/3/005.

[3] B. Gonzales, D. Spronk, Y. Cheng, et al. "Rectangular computed tomography using a stationary array of CNT emitters: initial experimental results". *Medical Imaging 2013: Physics of Medical Imaging*. Ed. by R. M. Nishikawa and B. R. Whiting. SPIE, 2013. DOI: 10.1117/12.2008030.

[4] G. Vogtmeier, J. Bredno, R. Pietig, et al. "Computed tomography scanner apparatus and method for ct-based image acquisition based on spatially distributed x-ray microsources of the cone-beam type". English. Pat. WO2009115982A1. 2009.

[5] H. K. Tuy. "An Inversion Formula for Cone-Beam Reconstruction". *SIAM Journal on Applied Mathematics* 43.3 (June 1983), pp. 546–552. DOI: 10.1137/0143035.

[6] S. Metzler, J. Bowsher, and R. Jaszczak. "Geometrical similarities of the Orlov and Tuy sampling criteria and a numerical algorithm for assessing sampling completeness". *IEEE Transactions on Nuclear Science* 50.5 (2003), pp. 1550–1555. DOI: 10.1109/tns.2003.817385.

[7] J. Lin and S. R. Meikle. "Truncated pinhole SPECT: Sufficient sampling criteria and applications". *IEEE Nuclear Science Symposium: Medical Imaging Conference*. IEEE, 2010. DOI: 10.1109/nssmic.2010.5874140.

[8] B. Liu, J. Bennett, G. Wang, et al. "Completeness map evaluation demonstrated with candidate next-generation cardiac CT architectures". *Medical Physics* 39.5 (2012), pp. 2405–2416. DOI: 10.1118/1.3700172.

[9] R. Clackdoyle and F. Noo. "Quantification of Tomographic Incompleteness in Cone-Beam Reconstruction". 4.1 (Jan. 2020), pp. 63–80. DOI: 10.1109/trpms.2019.2918222.

[10] F. Stopp, C. Winne, E. Jank, et al. "Quality evaluation of image recording strategies for limited angle tomography". *Tsinghua Science and Technology* 15.1 (2010), pp. 25–29. DOI: 10.1016/s1007-0214(10)70004-3.

[11] A. Gonzalez. "Measurement of Areas on a Sphere Using Fibonacci and Latitude–Longitude Lattices". *Mathematical Geosciences* 42.1 (2009), pp. 49–64. DOI: 10.1007/s11004-009-9257-x.

[12] S Rit, M. V. Oliva, S Brousmiche, et al. "The Reconstruction Toolkit (RTK), an open-source cone-beam CT reconstruction toolkit based on the Insight Toolkit (ITK)". *Journal of Physics: Conference Series* 489 (2014), p. 012079. DOI: 10.1088/1742-6596/489/1/012079.